

Conformational analysis of mixed oxathia crown ethers and their complexational ability towards Ag(I) and Pd(II)—an experimental solution NMR and theoretical molecular modelling study

Anja Holzberger, Hans-Jürgen Holdt and Erich Kleinpeter*

Universität Potsdam, Chemisches Institut, P.O. Box 69 15 53, D-14415 Potsdam, Germany

Received 12th February 2004, Accepted 8th April 2004

First published as an Advance Article on the web 19th May 2004

Both the conformation and flexibility of four mixed oxathia crown ethers and their Ag(I) and Pd(II) complexes were studied by ^1H NMR (δ , J , NOE, T_1), ^{13}C NMR, dynamic ^1H NMR spectroscopy and molecular modelling. The stoichiometry and stability constants of the complexes were determined from corresponding Job's plots in the case of Ag(I) complexes as the interchange between free and complexed states was fast on the NMR timescale; interchange for the Pd(II) complexes was sufficiently slow such that distinct sub-spectra were observable for the free and complexed states. In all cases where complexation was observed, 1 : 1 complexes were formed. Global minima structures determined from the modelling studies were analysed with respect to the barriers to ring interconversion, the flexibility of the species in solution and the preferred complexation of Ag(I) and Pd(II) to the sulfur atoms of the crown ethers.

Introduction

To reduce the flexibility of crown ethers, it is possible to insert rigid and/or voluminous structural fragments into the saturated crown ether moiety. This can also have the effect that the donor atoms are forced into arrangements that improve the ability of the crown to form complexes with certain metal cations. Mixed oxathia crown ethers are known to form complexes with *A*, *AB* and *B* class metal cations¹ and previous studies of maleonitrile dithia crown ethers have shown that mnXS_2O_n (mn = maleonitrile, X = number of atoms of the macrocyclic ring, $S_2 = 2$ sulfur atoms in the ring, $\text{O}_n = n$ oxygen atoms in the ring, $n = 2-5$) interacts with Ag(I) *via* both the oxygen and the sulfur donor atoms, whereas Bi(III) and Sb(III) are coordinated *via* the oxygen atoms only and Pd(II) and Pt(II) are coordinated *via* the sulfur atoms only.² The stability of these complexes was found to decrease in the following order of crown size: $\text{mn}12\text{S}_2\text{O}_2 > \text{mn}18\text{S}_2\text{O}_6 > \text{mn}15\text{S}_2\text{O}_3$. Additionally, it was found that the sulfur atoms can adopt different *E/Z*-configurations, with respect to the plane of the rigid maleonitrile moiety, depending on the ring size of the macrocycle.³

We now continue in this vein and herein report the detailed conformational and complexational study of four mixed oxathia crown ethers containing large aromatic subunits. The mixed oxathia crown ethers **1-4** are available by synthesis⁴ from their unsaturated parent compounds by substitution of the ethylene bridge between either two sulfur atoms or two oxygen atoms by voluminous aromatic subunits (see Fig. 1). Both the NMR investigations of the conformational flexibility of the free crowns as well as the complexational behaviour towards the transition metal cations Ag(I) and Pd(II) are reported. The NMR studies were also supported by molecular modelling calculations which afforded clear visualisation of the global minima structures.

Experimental

Syntheses

The mixed oxathia crown ethers **1** (mp 175–176 °C, yield 28%), **3** (mp 192–194 °C, yield 24%) and **4** (mp 169 °C, yield 34%) were obtained by dehydrohalogenation of dithiatriethylene glycol and the *ortho*-dichloro derivative of the respective aromatic subunit under high dilution conditions. Dehydro-

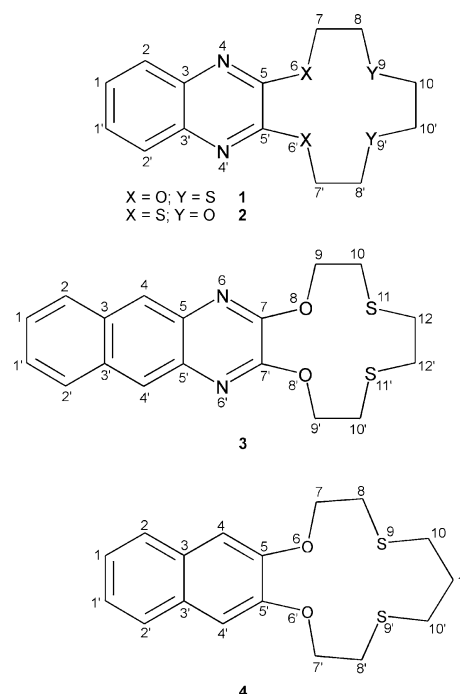


Fig. 1 The structure of the compounds **1-4** under study and the numbering system employed.

halogenation of the *ortho*-dithiol derivative of quinoxaline with 1,8-dichloro-3,6-dioxaoctane under high dilution conditions furnished compound **2** (mp 127–128 °C, yield 9.3%).⁴

NMR spectroscopy

^1H and ^{13}C NMR spectra were recorded on Bruker Avance 500 or 300 NMR spectrometers using 5 mm probes operating at 500 and 300 MHz for ^1H , respectively, and 125 and 75 MHz for ^{13}C , respectively. For all measurements, a 6 : 4 mixture of CD_2Cl_2 and CD_3CN was employed as the solvent using TMS as an internal reference (= 0 ppm for both nuclei). Signal assignment was performed at 298 K by utilisation of standard Bruker pulse sequences (^1H , ^{13}C , COSY, HMQC and HMBC).

For ^1H NMR spectra, the digital resolution was set to 16 data points Hz^{-1} and for ^{13}C spectra, to 1.6 data points Hz^{-1} . For 2D

Table 1 ^1H chemical shifts (δ/ppm) of **1–4** and the complexes formed with $\text{Ag}(\text{I})$ and $\text{Pd}(\text{II})$

	H-1	H-2	H-4	H-7	H-8	H-9	H-10	H-11	H-12
1	7.42	7.66	—	4.73	2.87	—	2.96	—	—
$[\mathbf{1}\cdot\text{Ag}(\text{I})]\text{BF}_4$	7.47	7.67	—	4.45	3.04	—	3.10	—	—
$[\mathbf{1}\cdot\text{Pd}(\text{II})](\text{BF}_4)_2$	—	—	—	5.01, 4.91	3.56, 3.27	—	3.27	—	—
2	7.57	7.84	—	3.41	3.60	—	3.21	—	—
$[\mathbf{2}\cdot\text{Pd}(\text{II})](\text{BF}_4)_2$	8.11	8.21	—	3.81, 3.45	3.89, 3.33	—	3.87	—	—
3	7.51	8.00	8.24	—	—	4.85	2.99	—	3.07
$[\mathbf{3}\cdot\text{Ag}(\text{I})]\text{BF}_4$	7.55	8.05	8.30	—	—	4.60	3.25	—	3.27
$[\mathbf{3}\cdot\text{Pd}(\text{II})](\text{BF}_4)_2$	7.62	8.13	8.45	—	—	4.98, 5.05	3.23, 3.53	—	3.29
4	7.33	7.66	7.05	4.31	3.04	—	2.82	2.32	—
$[\mathbf{4}\cdot\text{Pd}(\text{II})](\text{BF}_4)_2$	7.58	7.16	7.31	4.25, 4.29	3.37, 2.88	—	2.57, 1.83	1.96, 2.06	—

Table 2 ^{13}C chemical shifts (δ/ppm) of **1–4** and the complexes formed with $\text{Ag}(\text{I})$ and $\text{Pd}(\text{II})$

	C-1	C-2	C-3	C-4	C-5	C-7	C-8	C-9	C-10	C-11	C-12
1	127.1	126.5	137.6	—	150.0	70.2	31.7	—	34.3	—	—
$[\mathbf{1}\cdot\text{Ag}(\text{I})]\text{BF}_4$	127.3	126.4	137.2	—	150.3	68.2	33.0	—	35.7	—	—
$[\mathbf{1}\cdot\text{Pd}(\text{II})](\text{BF}_4)_2$	127.8	126.3	137.1	—	149.2	61.5	36.6	—	36.9	—	—
2	129.3	128.1	141.2	—	148.8	35.8	70.7	—	70.3	—	—
$[\mathbf{2}\cdot\text{Pd}(\text{II})](\text{BF}_4)_2$	135.6	130.1	141.5	—	146.5	42.2	66.4	—	63.1	—	—
3	128.5	125.9	136.1	124.8	132.5	150.4	—	70.3	31.7	—	34.4
$[\mathbf{3}\cdot\text{Ag}(\text{I})]\text{BF}_4$	125.4	127.0	134.8	123.5	131.5	140.9	—	67.2	32.7	—	35.5
$[\mathbf{3}\cdot\text{Pd}(\text{II})](\text{BF}_4)_2$	127.5	128.9	134.4	125.7	137.3	151.4	—	63.2, 63.8	39.0	—	39.6
4	124.2	126.3	128.9	106.7	148.6	70.6	31.7	—	33.3	31.0	—
$[\mathbf{4}\cdot\text{Pd}(\text{II})](\text{BF}_4)_2$	127.3, 127.1	128.5, 128.3	132.2, 132.7	116.4, 115.8	150.0, 150.5	69.0, 64.6	38.3, 39.3	—	30.5, 28.5	23.2	—

NOESY experiments, an optimal value for the mixing time τ_m was assessed as 400 ms. To avoid confusion arising from spin diffusion, 2D ROESY spectra were also recorded for comparison and also utilised mixing times of 400 ms. For both NOESY and ROESY experiments as well as the T_1 measurements, paramagnetic oxygen was displaced from the NMR solutions by ultrasonification for 30 minutes under argon prior to measurement. T_1 values were measured using the inversion recovery pulse sequence with a total of 16 different delay times. T_1 values were then calculated using standard Bruker software and are reported with an uncertainty of 5 ms. Vicinal ^1H – ^1H coupling constants were measured using the JRESQF pulse sequence where the spectral widths were set to 4125 and 40 Hz for the f_2 and f_1 dimensions, respectively, with digital resolutions of 4 and 0.2 Hz in f_2 and f_1 , respectively.

For the determination of the barriers to ring interconversion (ΔG^\ddagger), the rate constants k_c at the coalescence temperatures T_c were calculated from the chemical shift difference $\delta\nu$ of the respective peaks extrapolated to T_c using the Gutowski–Holm method ($k_c = 2.22\delta\nu$).⁵ Inserting the resulting rate constants into the Eyring equation [$\Delta G^\ddagger = 19.14T_c(10.32 + \lg(T_c/k_c))$] provided values of ΔG^\ddagger .⁶ Coalescence temperatures are reported with an uncertainty of 1 K.

Titration experiments were conducted using the continuous variation method⁷ as follows: stock solutions of AgBF_4 , $[\text{Pd}(\text{CH}_3\text{CN})_4](\text{BF}_4)_2$ and **1–4** were, for convenience, made up to the same concentration (3.3×10^{-4} M) to facilitate a simple procedure whereby the sum of the concentrations of the ligands and the metals was maintained as a constant (as it is required to be) during the course of the titration without any adjustment of the solutions. First, the ^1H NMR spectra of the free ligands were recorded. Following this, the concentration of the ligand was decreased successively whilst the concentration of the metal ion was increased accordingly (*i.e.* from **1** : $\text{AgBF}_4 = 9 : 1$ to **8** : **2** . . . to **1** : **9**, *etc.*).

Molecular modelling

Random search simulations were performed using the program SYBYL⁸ with the Tripos force field⁹ and consisted of 100,000 cycles. All torsional angles within the ring were allowed to vary

randomly and no constraints were applied. After each cycle, the optimised conformation was stored if the heat of formation was within 5 kcal mol⁻¹ of the lowest calculated heat of formation. The simulation was terminated prematurely if all so obtained conformations had been counted at least 5 times. This ensured that the global minimum was found with a confidence in excess of 95%.

The geometry optimisations of the free ligands were performed using the semiempirical method PM3¹⁰ and the $\text{Ag}(\text{I})$ and $\text{Pd}(\text{II})$ ion complexes with the semiempirical method ZINDO.¹¹ Calculations were performed on IRIS-INDIGO XS24 or SGI O2 workstations or on PCs with Pentium 1 processors.

Results and discussion

NMR of the free ligands

Signal assignment began with the carbon atoms of the aromatic unit linked closest to the aliphatic moiety as these resonances are shifted to lower field in comparison to the other ^{13}C resonances and exhibit long-range couplings to the methylene protons in close proximity to this rigid part of the molecule. The other signals were assigned successively by utilisation of the standard 2D NMR techniques COSY, HMQC and HMBC.

The ring interconversion is fast on the NMR timescale for all of **1–4** and only population-weighted averaged signals for both the protons as well as the carbon nuclei were obtained at room temperature (see Tables 1 and 2). Additionally, proton (and carbon) nuclei pairs on opposite sides of a plane perpendicular to and bisecting the aromatic moiety, are rendered equivalent and only a single resonance is exhibited for each such related pair. The observed vicinal coupling constants adopt values of 4.5–5 Hz in the O–CH₂–CH₂–S fragments of **1–4** and *ca.* 7 Hz in the S–CH₂–CH₂–CH₂ fragment of **4** indicating a rapid interconversion of the corresponding torsional angles but with a tendency towards angles providing synclinal relationships.

Upon lowering the temperature, the signals of all of the compounds broaden but only for **2** could decoalescence of the signals be obtained (given in Table 3). The signal for H-7 in **2** split into two signals at 244 K, whilst the signals for H-8 and

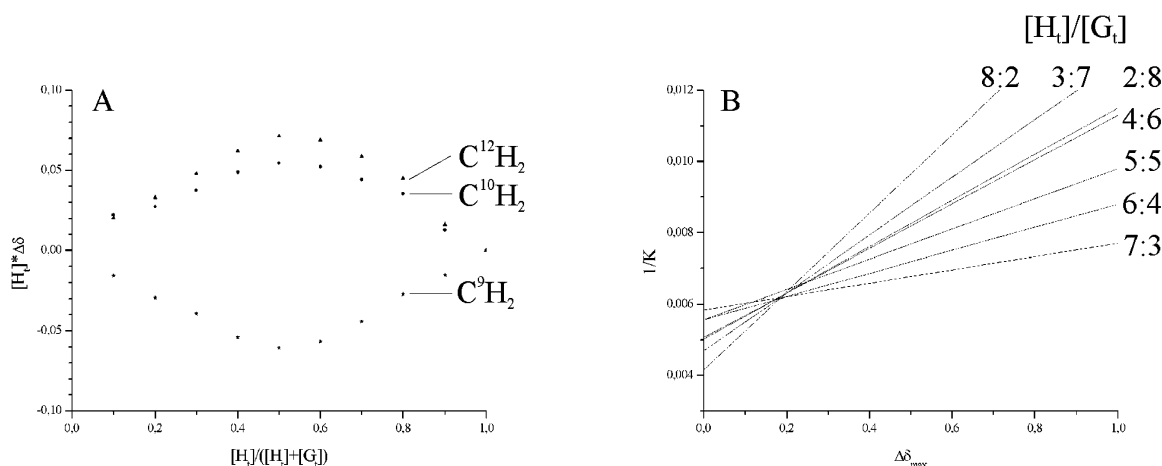


Fig. 2 Job's plot for the titration of **3** with AgBF_4 (A) and Rose–Drago plot for the determination of the stability constant of $[\mathbf{3}\cdot\text{Ag}(\text{t})]\text{BF}_4$ from the titration experiments.

Table 3 Coalescence temperatures T_c (K), chemical shift differences $\delta\nu$ (Hz) and activation barrier ΔG^\ddagger (kcal mol^{-1})

Compound	Observed protons	T_c (K)	$\delta\nu$ (Hz)	ΔG^\ddagger (kcal mol^{-1})
2	-C(7) H_2 -	244	190	12.1
	-C(8) H_2 -	230	210	11.0
	-C(10) H_2 -	230	51	11.1
1 -Ag(t)	-C(7) H_2 -	248	179	11.4
	-C(7) H_2 -	228	159	10.4
3 -Ag(t)	-C(7) H_2 -	216	145	10.5
	-C(7) H_2 -	180	—	—

H-10 split only upon reaching 230 K. The resulting barriers to interconversion were calculated as 12.1, 11.0 and 11.1 kcal mol^{-1} for H-7, H-8 and H-10, respectively. This trend indicates that the intramolecular flexibility increases with increasing distance from the quinoxaline unit in that molecule. However, below 230 K the split signals remained broad and J couplings could not be extracted to relay more information regarding the preferred conformation of **2**.

In the free ligands **1**, **3** and **4**, NOEs were not observed indicating that the C–X–C–C (X = O, S) torsional angles in the saturated parts of these molecules [C(7)–C(8)–S(9)–C(10) and C(8)–S(9)–C(10)–C(10')] in **1**, C(9)–C(10)–S(11)–C(12) and C(10)–S(11)–C(12)–C(12') in **3**, C(7)–C(8)–S(9)–C(10) and C(8)–S(9)–C(10)–C(11) in **4**] for the adopted conformations are such that they are in synclinal relationships. For compound **2**, an NOE was detected between H-8 and H-10. Although lacking a suitable pair of protons within the molecule for distance calibration, it was nevertheless assumed that the corresponding ^1H – ^1H distance does not exceed 3.0 Å. Therefore, at least one of the two torsional angles C(7)–C(8)–O(9)–C(10) or C(8)–O(9)–C(10)–C(10') in the C–C–O–C–C fragment must be such that they are in an antiperiplanar relationship.

NMR titration experiments

Two different phenomena for the complexation of either Ag(I) or Pd(II) were observed when performing the titration experiments. Upon the addition of AgBF_4 to the solutions of the ligands **1**–**4**, the chemical shifts of the ^1H and ^{13}C nuclei changed significantly but the interconversion between free and complexed ligands was fast on the NMR timescale and only population-weighted averages of the spectra for the two states were observed. Hence, Job's plots⁷ were required to be constructed to determine both the stoichiometry and the stability constants of the metal–ligand complexes that were formed. From the plot of $[\text{H}_i](\Delta\delta)$ vs. $[\text{H}_i]/([\text{H}_i] + [\text{G}_i])$, the metal-to-ligand ratio of the complexes was inferred by the value of the x-coordinate at the plot azimuth (*cf.* Fig. 2A). Stability con-

stants were calculated using the Rose–Drago equation.¹² The total concentration of host $[\text{H}_i]$ and metal $[\text{G}_i]$ is known and population-weighted averages of chemical shifts $\Delta\delta$ at the various titration steps were determined. Then, a series of lines with varying $\Delta\delta_{\text{max}}$ is obtained and the corresponding reciprocal stability constant could be calculated with the Rose–Drago equation. The procedure was repeated for another titration step. At the intersection of both lines the reciprocal stability constant and the chemical shift difference between the free and the complexed ligand is observed (*cf.* Fig. 2 for **3**; the same plots were established for **1**).

$$\frac{1}{K} = ([\text{H}_i]\Delta\delta_{\text{max}} - [\text{H}_i]\Delta\delta) * \left(\frac{[\text{G}_i]}{[\text{H}_i]\Delta\delta} - \frac{1}{\Delta\delta_{\text{max}}} \right)$$

K = stability constant, $[\text{H}_i]$ = total concentration of the host, $[\text{G}_i]$ = total concentration of the metal, $\Delta\delta$ = variation of the chemical shift at a defined titration step, $\Delta\delta_{\text{max}}$ = chemical shift difference between the free and the complexed state of the ligand.

From these Job's plots it was determined that **1** and **3** both form 1 : 1 complexes with Ag(I) whereas **2** and **4** do not exhibit complexation. The silver complexes of **1** and **3**, though, are rather weak: stability constants ($\log K$) of 3.45 for $[\mathbf{1}\cdot\text{Ag}(\text{t})]\text{BF}_4$ and 3.20 for $[\mathbf{3}\cdot\text{Ag}(\text{t})]\text{BF}_4$ were calculated. Electron-withdrawing of the aromatic moiety in **2** reduces the donating ability of the sulfur atoms attached to this part of the molecule, therefore no coordination to Ag(I) occurs. Similar results were obtained by Lange and co-workers when studying 14-membered maleonitrile tetrathia crown ethers.¹³

In contrast to complexation with Ag(I), a second set of signals was obtained upon the addition of $[\text{Pd}(\text{CH}_3\text{CN})_4](\text{BF}_4)_2$ to the solutions of the ligands indicating slow exchange between the free and complexed states on the NMR timescale. The intensities of the signals arising from the Pd complex were observed to increase with the amount of Pd salt added, and simultaneously, the intensities of the signals arising from the free ligand decreased. These latter signals disappeared altogether when a metal-to-ligand ratio of 1 : 1 was reached. Due to serious overlap of the signals of the free and complexed ligands, however, it was not possible to calculate the stability constants directly from the ^1H NMR spectrum; instead HMQC experiments were performed to separate the signals. The stability constants of the Pd(II) complexes were calculated with the following equation:¹²

$$K = \frac{\frac{I_c}{I_c + I_l} * [\text{H}_i]}{\left([\text{H}_i] - \frac{I_c}{I_c + I_l} * [\text{H}_i] \right) * \left([\text{G}_i] - \frac{I_c}{I_c + I_l} * [\text{H}_i] \right)}$$

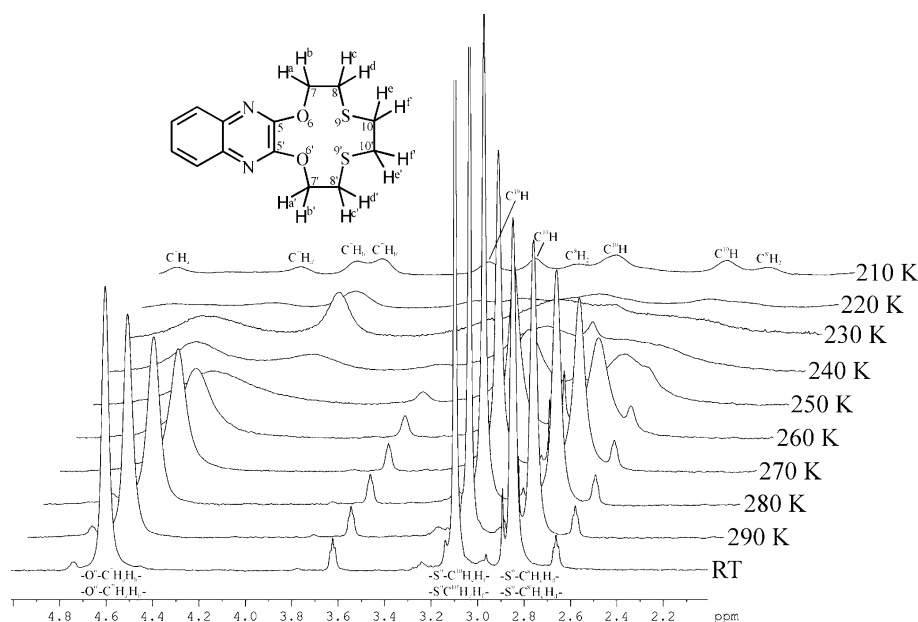


Fig. 3 The ^1H NMR of the complex $[\mathbf{1}\cdot\text{Ag}(\text{I})]\text{BF}_4$ over the range of 210 K to RT.

K = stability constant, I_C = intensity of the proton signal of the complex, I_L = intensity of the proton signal of the free ligand, $[\text{H}_L]$ = total concentration of the ligand, $[\text{G}_L]$ = total concentration of the metal.

For the Pd(II) complexes of ligands **1-4** the following stability constants were estimated: $\lg K = 4.20$ (**1**-Pd(II)), 3.61 (**2**-Pd(II)), 3.82 (**3**-Pd(II)) and $\lg K = 3.53$ (**4**-Pd(II)).

Common to all the complexes that were formed was the observation that the resonances of the methylene groups linked closest to the sulfur atoms were shifted downfield (+0.14 to +0.26 ppm in Ag(I) complexes and +0.04 to 0.69 ppm in Pd(II) complexes) in comparison to the resonances of the free ligands. The signals from the methylene groups attached to the oxygen atoms, contrastingly, were shifted to higher field (−0.25 to −0.28 ppm in Ag(I) and −0.02 to −0.27 ppm in Pd(II) complexes, respectively). Evidently, both the Ag(I) and Pd(II) cations are only coordinated *via* the sulfur atoms of the crowns.

NMR of the complexes with Ag(I)

Due to the rapid interconversion of the ligand between the free and the complexed state, only population-weighted averages of the signals were obtained, and these resulted from an unknown number of conformations that participate in the conformational equilibrium. However, as for the free ligands, the vicinal coupling constants ($^3J_{\text{H,H}}$) of the Ag(I) complexes remained in the range of 4.5–5 Hz, indicating that the donor atoms in the free ligand were predisposed for the complexation of Ag(I), at least in the case of **1** and **3**. Nonetheless, the intramolecular flexibility is reduced within the complete macrocyclic ring due to complexation as shown by comparison of the T_1 s for the ^1H s of the ligands in the free and the complexed states (see Table 4). T_1 s are reflective of the mobility of a molecule as a whole and its internal flexibility as a sum parameter, *i.e.* smaller T_1 values indicate reduced flexibility.

Additionally, differences in flexibility between different structures are also evident, *viz.* the intramolecular mobility of the Ag(I) complex of **1** is lower than that of the Ag(I) complex of **3**. While the flexibility of the $-\text{S}^9-\text{C}^{10}\text{H}_2-\text{C}^{10}\text{H}_2-\text{S}^{10}-$ moiety in **1**-Ag(I) (T_1 1.02 s) and of $-\text{S}^{11}-\text{C}^{12}\text{H}_2-\text{C}^{12}\text{H}_2-\text{S}^{11}-$ in **3**-Ag(I) (T_1 1.01 s) is equal, we obtained a higher intramolecular mobility for the $-\text{S}^8-\text{C}^9\text{H}_2-\text{C}^{10}\text{H}_2-$ fragment in **3**-Ag(I) (T_1 1.49 s for C^9H_2 , T_1 0.97 s for C^{10}H_2) compared

Table 4 Spin-lattice relaxation times (T_1 /s) for selected protons of **1-4** and the complexes formed with Ag(I) and Pd(II)

	H-7	H-8	H-9	H-10	H-11	H-12
1	2.15	1.55	—	1.68	—	—
1 ·Ag(I)BF ₄	0.83	0.82	—	1.02	—	—
1 ·Pd(II)(BF ₄) ₂	0.53	0.59	—	—	—	—
2	1.75	1.96	—	1.74	—	—
2 ·Pd(II)(BF ₄) ₂	0.69	0.68	—	0.66	—	—
3	—	—	1.70	1.25	—	1.23
3 ·Ag(I)BF ₄	—	—	1.49	0.97	—	1.01
3 ·Pd(II)(BF ₄) ₂	—	—	0.42	—	—	—
4	1.15	1.25	—	1.30	1.29	—
4 ·Pd(II)(BF ₄) ₂	0.63	0.57	—	0.60	—	—

with the $-\text{S}^6-\text{C}^7\text{H}_2-\text{C}^8\text{H}_2-$ fragment in **1**-Ag(I) (T_1 0.83 s for C^7H_2 , T_1 0.82 s for C^8H_2). This is due to the reduced stability of **3**-Ag(I) compared with the **1**-Ag(I) complex.

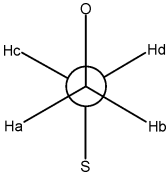
This result is corroborated by dynamic NMR experiments on these complexes; whereas the only signal decoalescence of the Ag(I) complex of **3** was obtained at 180 K (splitting of the $-\text{O}-\text{CH}_2-$ signals), the NMR spectra of the Ag(I) complex of **1** exhibited rather complex changes at lower temperatures (*cf.* Fig. 3). The signals from the $-\text{O}-\text{CH}_2-$ groups of **1** actually split three times, at 248, 228 and 216 K. The calculated corresponding barriers to ring interconversion were very similar: 11.4, 10.4 and 10.5 kcal mol^{−1}, respectively. In the temperature range 240–224 K, the proton resonances of the $-\text{S}-\text{CH}_2-$ groups also decoalesced, but the resulting peaks overlapped and energy values could not be determined. Even at 180 K the peaks remained broad thereby precluding the extraction of $^1\text{H}-^1\text{H}$ coupling constants.

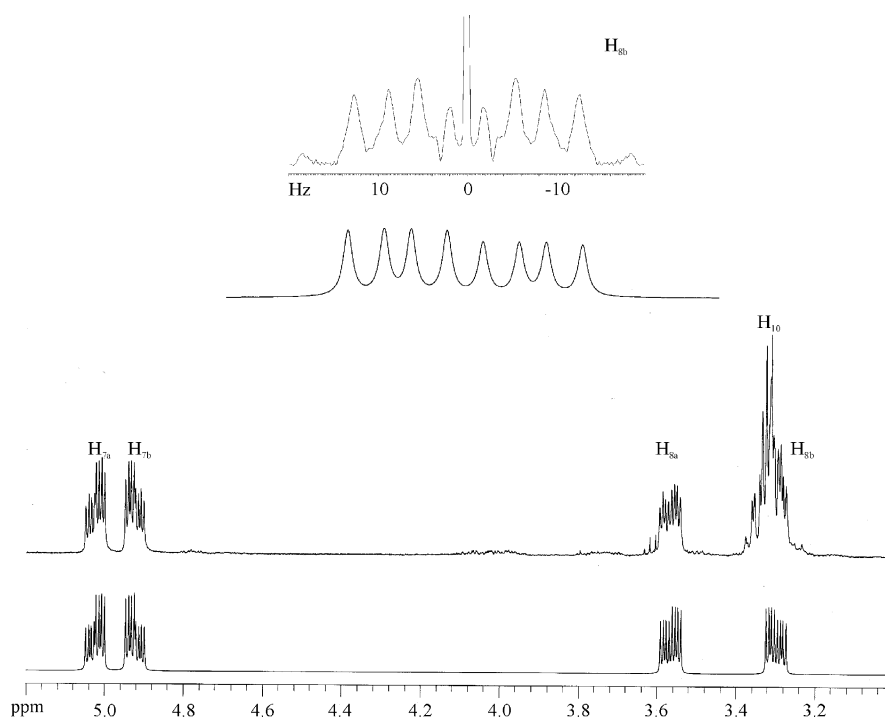
As in the free ligands, NOEs could not be obtained for the complexes meaning that there was no alteration of the C–S–C–C dihedral angles due to the complexation of Ag(I). This result serves as further evidence for the predisposition of the donor atoms of the ligand for the complexation of Ag(I) ions in the cases of **1** and **3**.

NMR of the complexes with Pd(II)

For the Pd complexes of **1-4**, their flexibility is decreased by a relatively greater amount compared to the corresponding loss

Table 5 Selected vicinal ^1H - ^1H coupling constants ($^3J_{\text{H,H}}/\text{Hz}$) extracted for the Pd(II) complexes of **1-4** and calculated S-C-C-O torsional angle ($^\circ$)

	$^3J_{\text{Ha,Hc}}$	$^3J_{\text{Ha,Hd}}$	$^3J_{\text{Hb,Hc}}$	$^3J_{\text{Hb,Hd}}$	SCCO torsional angle
[1 ·Pd(II)](BF ₄) ₂	3.8	6.9	7.1	3.9	127, 244
[2 ·Pd(II)](BF ₄) ₂	8.0	2.9	7.9	3.0	30, 150
[3 ·Pd(II)](BF ₄) ₂	3.8	6.9	7.1	3.9	129, 242
[4 ·Pd(II)](BF ₄) ₂	8.9	2.0	4.7	2.2	129, 314

**Fig. 4** Experimental (upper trace) and simulated (lower trace) ^1H NMR spectra of the O-C-C-S fragment of the Pd(II) complex of **1**.

of flexibility due to Ag(I) complexation. Therefore, the Pd(II) complexes of **1-4** must be more stable by comparison. Moreover, due to complexation, the plane of equivalence through time-averaged motion is lost and some of the methylene protons are rendered distinct. Split resonances for the $-\text{CH}_2-$ protons linked closest to the aromatic subunits were obtained for all the compounds **1-4**, and dependent on the flexibility, also for some or all of the remaining $-\text{CH}_2-$ groups. For the ^{13}C resonances, only for the Pd complexes of **3** and **4** did additional signals appear in the spectra.

Since the Pd(II) ion interacts strongly with the sulfur atoms of the ligands and not the oxygens (*vide supra*), the methylene groups attached to the oxygens remain fairly flexible. Nevertheless, the reduction of intramolecular mobility enabled analysis of the ^1H - ^1H coupling patterns ($^3J_{\text{H,H}}$) of the O-C-C-S fragments of the ligands by extraction of the multiplets using 2D J-resolved spectra, thus enabling conclusions to be drawn regarding the preferred conformations of the Pd(II) complexes. Simulation of the experimental spectra was performed by variation of the geminal and vicinal ^1H - ^1H coupling constants and calculation of the resulting spectrum using the simulation tool of the NMR software package MestRe-C¹⁴ (*cf.* Fig. 4).

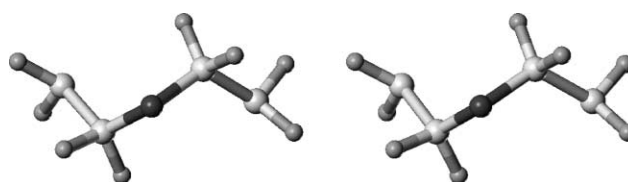
The extracted $^3J_{\text{H,H}}$ coupling constants (Table 5) were used to calculate the corresponding H-C-C-H torsional angles *via* the Karplus equation¹⁵ implemented in the Altona program.¹⁶ The evaluation of all possible H-C-C-H torsional angles in the spin system $-\text{CH}_2-\text{CH}_2-$ led to the conclusion that the

O-C-C-S dihedral angles in **1** and **3** are indicative of anticlinal relationships and syn- or anticlinal relationships in **2** and **4**. Thus the annelated aromatic moieties proved to be of influence on the complexation of Pd(II) and the stability of the corresponding complexes but not on their geometry.

NOE experiments on the Pd(II) complexes

In order to glean more information on the stereochemistry of the ligands in the Pd(II) complexes (*i.e.* ^1H - ^1H distances), 2D NOESY spectra were again recorded. For the Pd(II) complex of **2**, NOEs were not detected. This means that, like in the free ligand, the C-O-C-C torsional angles are in synclinal relationships to gain maximum distance between the methylene protons (*cf.* Fig. 5). For the Pd complexes of **1** and **3**, only one stereochemically interesting NOE was obtained (*cf.* Fig. 6).

For the Pd(II) complex of **4**, several NOEs were obtained (*cf.* Fig. 6). The distance between protons H-2 and H-4 is fixed

**Fig. 5** Conformation of the C(7)-C(8)-O(9)-C(10)-C(10') fragment for the palladium complex of **2** (relaxed view).

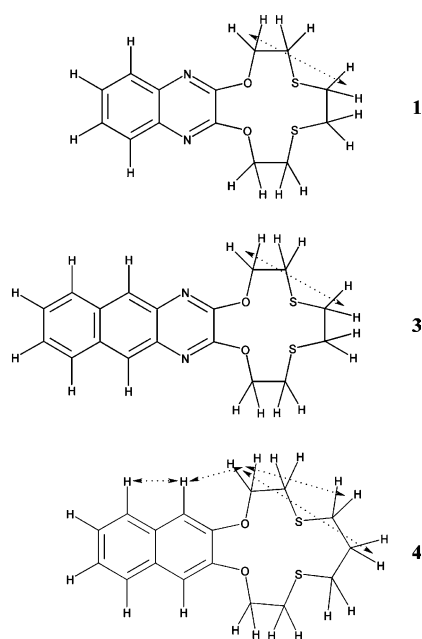


Fig. 6 Observed NOEs for the Pd(II) complexes of **1**, **3** and **4**.

and could potentially be used for calibration of other ^1H - ^1H distances, however, due to errant variation of the integrated volumes of the cross peaks, the resulting calculated values were rendered meaningless. Therefore, the corresponding ^1H - ^1H distances for detected NOEs were assumed not to exceed 3.0 Å. In the Pd(II) complex of **4**, additional NOEs between the following proton pairs were detected: H-4, H-7; H-7, H-10 and H-7, H-11. This combination is possible when the corresponding methylene groups are located on the same side of the theoretical plane passing through the donor atoms and when the coordinated Pd(II) ion is located on the opposite side of this plane.

Molecular modelling of the free ligands

The information provided by the NMR experiments regarding the geometry of the ligands in both the free and the complexed states was used to limit the number of conformations resulting from random search calculations. Using the random search method without any constraints provided a large number of possible conformations for the free ligands possessing energies within 3 kcal mol $^{-1}$ of the global minimum in each case (18 for **1**, 12 for **2**, 16 for **3** and 64 for **4**), thus implying that they can participate in the conformational equilibrium. The number of conformers per compound, however, is in qualitative agreement with the results of the dynamic NMR measurements; only for **2** could ring interconversion be frozen (the lowest number of geometries was found for this compound), the signals of the other compounds, **1**, **3** and **4**, did not decoalesce and only line broadening was observed. Inclusion of the experimental result that the S-C-C-O torsional angles indicate synclinal over antiperiplanar arrangements leads to a reduction of the possible number of conformations for **1** and **2**, 11 in both cases, whilst the numbers of conformations for **3** and **4** remain invariant at 16 and 64, respectively. However, the other experimental observation that the C-S-C-C torsional angles in **1**, **3** and **4** indicate synclinal relationships reduces the number of possible geometries further for these three compounds, to 5, 5 and 7, respectively. In a like manner, the number of conformations for **2** is reduced to 5 because at least one C-O-C-C dihedral angle in the C-C-O-C-C fragment of this compound must be in an antiperiplanar arrangement. The most stable conformations for **1**-**4** are depicted in Fig. 7.

In all of these conformations the X-C=C-X fragment remains planar. The C=C-O-C dihedral angle in **1**, **3** and **4**

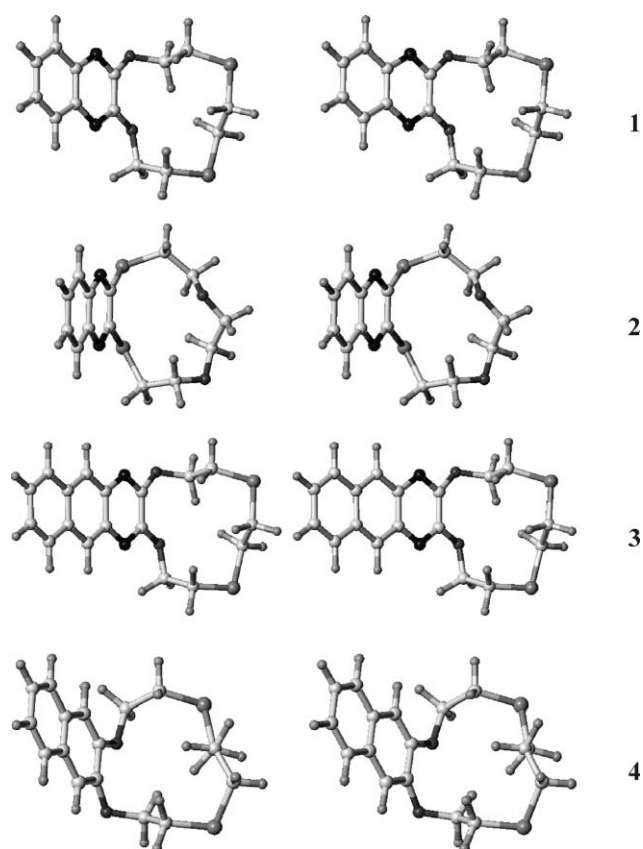


Fig. 7 Global minima structures of compounds **1**-**4** (stereo view).

results in synclinal or antiperiplanar arrangements whereas in the more rigid compound **2**, the C=C-S-C dihedral angle indicates a synclinal or anticlinal arrangement. The S-C-C-S fragments in **1** and **3** prefer antiperiplanar arrangements whilst the O-C-C-O fragments in **2** prefer an anticlinal relationship. The S-C-C-C torsional angle in **4** proved to occupy preferably the antiperiplanar orientation. Therefore the distance between the sulfur atoms is extended with respect to the sulfur-sulfur distances in **1** and **3**. This might be the reason therefore that no complex formation could be observed of **4** with the silver(I) ion.

Molecular modelling of the Ag(I) and Pd(II) complexes

Since the titration experiments provided the stoichiometry of the complexes and the chemical shift changes together with the T_1 measurements revealed the location of the complexed metal ions, *viz.* that they are coordinated *via* the sulfur atoms only, a Ag(I) or Pd(II) ion was placed above the crown ether ring in **1**-**4** in proximity to the sulfur atoms. The geometries obtained for the global minima of the free ligands were used as the starting structures for the calculations and the structures were then re-optimised using the semiempirical method ZINDO.¹¹ It was found that the number of possible conformations was reduced due to complexation with the metal cations. For the silver complexes of the ligands **1** and **3**, 4 identical conformations were found that matched the results of the NMR experiments. The number of conformations for the Pd complexes was reduced to 2 for **1**-**3** and to 1 for **4** (see Fig. 8).

This is in agreement with both the dynamic NMR experiments as well as the relaxation time measurements. In all of these conformations the cations are coordinated in the half-sandwich form and the complete macrocyclic ring is located on one side of the plane through the aromatic unit. In **1** and **3**, the S-C-C-S torsional angles alter from antiperiplanar to synclinal due to complexation, whereas in **2** the sulfur atoms are fixed in a synperiplanar relationship due to the rigidity of the proximal aromatic moiety.

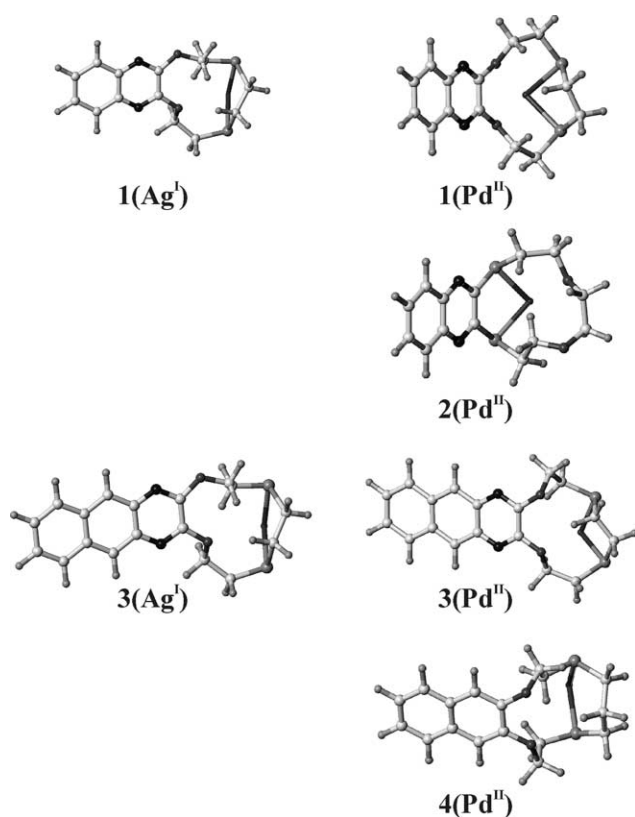


Fig. 8 Global minima structures of the Ag(I) and Pd(II) complexes of 1–4.

Conclusions

The global minima structures and the intramolecular flexibility of the mixed oxathia crown compounds 1–4 and their 1 : 1 complexes with Ag(I) and Pd(II) were studied by NMR spectroscopy (including dynamic NMR, titration experiments and T_1 and NOE measurements) and accompanying molecular modelling studies at the semiempirical level. In the complexes, both Ag(I) and Pd(II) ions are coordinated *via* the sulfur atoms of the crowns only. Due to complexation, the flexibility of the ligands is clearly reduced. Structural parameters (NOEs, $^3J_{\text{H,H}^{\text{S}}}$) were used to refine the results of the molecular modelling calculations and to derive the global minima geometries of the free ligands 1–4 as well as of their Ag(I) and Pd(II) complexes.

Acknowledgements

Dr Karel D. Klika is thanked for language correction and further assistance in the preparation of the manuscript.

References

- (a) H.-J. Drexler, H. Reinke and H.-J. Holdt, *Chem. Ber.*, 1996, **129**, 807; (b) H.-J. Drexler, M. Grotjahn, H.-J. Holdt and E. Kleinpeter, *Inorg. Chim. Acta*, 1999, **285**, 305; (c) H.-J. Drexler, I. Starke, M. Grotjahn, H. Reinke, E. Kleinpeter and H.-J. Holdt, *Z. Naturforsch., Teil B*, 1999, **54**, 799.
- E. Kleinpeter, M. Grotjahn, K. D. Klika, H.-J. Drexler and H.-J. Holdt, *J. Chem. Soc., Perkin Trans. 2*, 2001, 988.
- (a) H.-J. Drexler, I. Starke, M. Grotjahn, H.-J. Holdt and E. Kleinpeter, *Inorg. Chim. Acta*, 2001, **317**, 133; (b) M. Grotjahn, N. Jäger, H.-J. Drexler, H.-J. Holdt and E. Kleinpeter, *J. Mol. Model.*, 1999, **5**, 72.
- (a) S. Potratz, H.-J. Holdt, *Sulfur Lett.*, to be submitted; (b) S. Potratz, Diploma Thesis, University of Potsdam, 2002.
- H. S. Gutowski and C. H. Holm, *J. Chem. Phys.*, 1956, **25**, 1228.
- H. Friebolin, in *Ein- und zweidimensionale NMR-Spektroskopie*, VCH Publishers Inc., Weinheim, 1988.
- (a) Y. Shibata, B. Inoue and Y. Nakatuka, *Nippon Kagaku Kaishi*, 1921, **42**, 983; (b) R. Tsuchida, *Bull. Chem. Soc. Jpn.*, 1935, **10**, 27; (c) P. Job, *Comp. Rend.*, 1925, **180**, 928; (d) P. Job, *Ann. Chim. Phys.*, 1928, **9**, 113.
- SYBYL Molecular Modelling Software, Version 6.9, 2003, Tripos Inc., St. Louis, Missouri, USA.
- M. Clark, R. D. Cramer III and N. J. van Opdenbosch, *Comput. Chem.*, 1989, **10**, 982.
- J. J. P. Stewart, *J. Comput. Chem.*, 1981, **10**, 209.
- (a) M. Zerner, G. H. Loew, R. F. Kirchner and U. T. Mueller-Westerhoff, *J. Am. Chem. Soc.*, 1980, **102**, 589; (b) W. P. Anderson, W. D. Edwards and M. C. Zerner, *Inorg. Chem.*, 1986, **25**, 2728; (c) M. C. Zerner, in *Reviews in Computational Chemistry II*, VCH Publishers Inc., Weinheim, 1991, Ch. 8, pp. 313–365; (d) A. D. Bacon and M. C. Zerner, *Theor. Chim. Acta*, 1979, **53**, 2; (e) W. P. Anderson, T. R. Cundari and M. C. Zerner, *Int. J. Quantum Chem.*, 1991, **39**, 31.
- (a) N. J. Rose and R. S. Drago, *J. Am. Chem. Soc.*, 1959, **81**, 6138; (b) S. Nagakura, N. I. Nakano and T. Higuchi, *J. Am. Chem. Soc.*, 1958, **80**, 520; (c) K. Hirose, *J. Inclusion Phenom.*, 2001, **39**, 193.
- S. J. Lange, J. W. Sibert, C. L. Stern, A. G. M. Barrett and B. M. Hoffman, *Tetrahedron*, 1995, **51**, 8175.
- MestRe-C 2.3a, Magnetic Resonance Companion, Universidad de Santiago, 2000.
- C. A. G. Haasnoot, F. A. A. M. de Leew and C. Altona, *Tetrahedron*, 1980, **36**, 2783.
- C. M. Cerda-Garcia-Rojas, L. G. Zepeda and P. Joseph-Nathan, *Tetrahedron Comput. Methodol.*, 1990, **3**, 113.